Biomedical Optics EXPRESS

Diagnosis of oral precancer with optical coherence tomography

Cheng-Kuang Lee,[1] Ting-Ta Chi,[1] Chiung-Ting Wu,[1] Meng-Tsan Tsai,[2] Chun-Pin Chiang,[3] and Chih-Chung (C. C.) Yang[1,4,*]

[1]*Institute of Photonics and Optoelectronics, National Taiwan University, 1, Roosevelt Road, Section 4, Taipei, 10617 Taiwan*

[2]*Department of Electrical Engineering, Chang Gung University, 259, Wen-Hwa 1st Road, Kwei-Shan, Tao-Yuan, 33302 Taiwan*

[3]*Graduate Institute of Oral Biology and National Taiwan University Hospital, National Taiwan University, 1, Chang-Te St., Taipei, 10048 Taiwan*

[4]*Department of Electrical Engineering, National Taiwan University, 1, Roosevelt Road, Section 4, Taipei, 10617 Taiwan*

**ccy@cc.ee.ntu.edu.tw*

Abstract: A procedure for computer analyzing an optical coherence tomography (OCT) image of normal and precancerous oral mucosae is demonstrated to reasonably plot the boundary between epithelium (EP) and lamina propria (LP) layers, determine the EP thickness, and estimate the range of dysplastic cell distribution based on standard deviation (SD) mapping. In this study, 54 normal oral mucosa, 39 oral mild dysplasia, and 44 oral moderate dysplasia OCT images are processed for evaluating the diagnosis statistics. Based on SD mapping in an OCT image, it is found that the laterally average range percentages of 70% SD maximum level in the EP layer is a reasonably good threshold for differentiating moderate dysplasia from mild dysplasia oral lesion based on the OCT image analysis. The sensitivity and specificity in diagnosis statistics can reach 82 and 90%, respectively.

© 2012 Optical Society of America

OCIS codes: (110.4500) Optical coherence tomography; (170.3880) Medical and biological imaging.

References and links

1. A. Jemal, T. Murray, E. Ward, A. Samuels, R. C. Tiwari, A. Ghafoor, E. J. Feuer, and M. J. Thun, "Cancer statistics, 2005," CA Cancer J. Clin. **55**(1), 10–30 (2005).
2. M. Lingen, E. M. Sturgis, and M. S. Kies, "Squamous cell carcinoma of the head and neck in nonsmokers: clinical and biologic characteristics and implications for management," Curr. Opin. Oncol. **13**(3), 176–182 (2001).
3. "WHO Disease and injury country estimates," World Health Organization, 2009, *http://www.who.int/healthinfo/global_burden_disease/estimates_country/en/index.html*
4. B. W. Neville, D. D. Damm, C. M. Allen, and J. E. Bouquot, "Epithelial Pathology," in: B. W. Neville, D. D. Damm, C. M. Allen, and J. E. Bouquot, eds., *Oral and Maxillofacial Pathology*, 3rd ed. (Philadelphia, Sauders Elsevier, 2009), pp. 388–398.
5. E. S. Matheny, N. M. Hanna, W. G. Jung, Z. Chen, P. Wilder-Smith, R. Mina-Araghi, and M. Brenner, "Optical coherence tomography of malignancy in hamster cheek pouches," J. Biomed. Opt. **9**(5), 978–981 (2004).
6. P. Wilder-Smith, W. G. Jung, M. Brenner, K. Osann, H. Beydoun, D. Messadi, and Z. Chen, "*In vivo* optical coherence tomography for the diagnosis of oral malignancy," Lasers Surg. Med. **35**(4), 269–275 (2004).
7. A. L. Clark, A. Gillenwater, R. Alizadeh-Naderi, A. K. El-Naggar, and R. Richards-Kortum, "Detection and diagnosis of oral neoplasia with an optical coherence microscope," J. Biomed. Opt. **9**(6), 1271–1280 (2004).
8. J. M. Ridgway, W. B. Armstrong, S. Guo, U. Mahmood, J. Su, R. P. Jackson, T. Shibuya, R. L. Crumley, M. Gu, Z. Chen, and B. J. Wong, "*In vivo* optical coherence tomography of the human oral cavity and oropharynx," Arch. Otolaryngol. Head Neck Surg. **132**(10), 1074–1081 (2006).
9. M. DeCoro and P. Wilder-Smith, "Potential of optical coherence tomography for early diagnosis of oral malignancies," Expert Rev. Anticancer Ther. **10**(3), 321–329 (2010).
10. W. Jerjes, T. Upile, B. Conn, Z. Hamdoon, C. S. Betz, G. McKenzie, H. Radhi, M. Vourvachis, M. El Maaytah, A. Sandison, A. Jay, and C. Hopper, "*In vitro* examination of suspicious oral lesions using optical coherence tomography," Br. J. Oral Maxillofac. Surg. **48**(1), 18–25 (2010).

#165178 - $15.00 USD Received 21 Mar 2012; revised 29 May 2012; accepted 14 Jun 2012; published 18 Jun 2012
(C) 2012 OSA

11. P. Wilder-Smith, K. Lee, S. Guo, J. Zhang, K. Osann, Z. Chen, and D. Messadi, "*In vivo* diagnosis of oral dysplasia and malignancy using optical coherence tomography: preliminary studies in 50 patients," Lasers Surg. Med. **41**(5), 353–357 (2009).
12. C. S. Kim, P. Wilder-Smith, Y. C. Ahn, L. H. L. Liaw, Z. Chen, and Y. J. Kwon, "Enhanced detection of early-stage oral cancer *in vivo* by optical coherence tomography using multimodal delivery of gold nanoparticles," J. Biomed. Opt. **14**(3), 034008 (2009).
13. N. Ozawa, Y. Sumi, C. Chong, and T. Kurabayashi, "Evaluation of oral vascular anomalies using optical coherence tomography," Br. J. Oral Maxillofac. Surg. **47**(8), 622–626 (2009).
14. P. Wilder-Smith, M. J. Hammer-Wilson, J. Zhang, Q. Wang, K. Osann, Z. Chen, H. Wigdor, J. Schwartz, and J. Epstein, "*In vivo* imaging of oral mucositis in an animal model using optical coherence tomography and optical Doppler tomography," Clin. Cancer Res. **13**(8), 2449–2454 (2007).
15. M. T. Tsai, H. C. Lee, C. W. Lu, Y. M. Wang, C. K. Lee, C. C. Yang, and C. P. Chiang, "Delineation of an oral cancer lesion with swept-source optical coherence tomography," J. Biomed. Opt. **13**(4), 044012 (2008).
16. C. C. Yang, M.-T. Tsai, H.-C. Lee, C.-K. Lee, C.-H. Yu, H.-M. Chen, C.-P. Chiang, C.-C. Chang, Y.-M. Wang, and C. C. Yang, "Effective indicators for diagnosis of oral cancer using optical coherence tomography," Opt. Express **16**(20), 15847–15862 (2008).
17. M. T. Tsai, C. K. Lee, H. C. Lee, H. M. Chen, C. P. Chiang, Y. M. Wang, and C. C. Yang, "Differentiating oral lesions in different carcinogenesis stages with optical coherence tomography," J. Biomed. Opt. **14**(4), 044028 (2009).
18. C. K. Lee, M. T. Tsai, H. C. Lee, H. M. Chen, C. P. Chiang, Y. M. Wang, and C. C. Yang, "Diagnosis of oral submucous fibrosis with optical coherence tomography," J. Biomed. Opt. **14**(5), 054008 (2009).
19. M. C. G. Aalders, M. Triesscheijn, M. Ruevekamp, M. de Bruin, P. Baas, D. J. Faber, and F. A. Stewart, "Doppler optical coherence tomography to monitor the effect of photodynamic therapy on tissue morphology and perfusion," J. Biomed. Opt. **11**(4), 044011 (2006).
20. M. Yamanari, M. Miura, S. Makita, T. Yatagai, and Y. Yasuno, "Phase retardation measurement of retinal nerve fiber layer by polarization-sensitive spectral-domain optical coherence tomography and scanning laser polarimetry," J. Biomed. Opt. **13**(1), 014013 (2008).
21. B. Cense, T. C. Chen, B. H. Park, M. C. Pierce, and J. F. de Boer, "Thickness and birefringence of healthy retinal nerve fiber layer tissue measured with polarization-sensitive optical coherence tomography," Invest. Ophthalmol. Vis. Sci. **45**(8), 2606–2612 (2004).

1. Introduction

Oral cancer is among the ten most common cancers in the world. In the year of 2005, oral cancer occurs with an annual incidence of approximately 29,370 cases in the United States [1] and is the fifth most common cancer in the world [2]. Then, in the year of 2008, the death number caused by oral cancer was 95,400 for the male with age between 15 and 59 in the whole world [3]. This number ranks the fourth among various cancers. Squamous cell carcinoma (SCC) is the most common cancer in the oral cavity. It may evolve from oral mucosal lesions with benign epithelial hyperplasia (EH), mild dysplasia (MiD), moderate dysplasia (MoD), severe dysplasia, or carcinoma *in situ*. EH and MiD are relatively reversible lesions. Compared to patients with MoD or more severe lesions, patients with EH or MiD may have more chance to return to the healthy condition if they stop their harmful oral habits, including cigarette smoking, alcohol consumption, and areca quid chewing. However, if an oral lesion evolves into the MoD or severe dysplasia stage, it has relatively higher risk to further develop into an early-stage SCC and then a well-developed SCC if none of effective medical treatments is taken [4].

At the beginning of oral precancer development, dysplastic cells start to develop from the bottom of the epithelium (EP). Oral lesions are diagnosed as having MiD, MoD or severe dysplasia, when enough dysplastic cells are present in the basal one-third, in the basal two-thirds, or in more than the basal two-thirds but not the complete layer of the oral EP, respectively. In addition, oral lesions are diagnosed as having carcinoma *in situ* when the dysplastic cells occupy the entire EP layer. During the precancerous stages, the EP thickness may also increase. Beyond the stage of carcinoma *in situ*, the basement membrane, i.e., the boundary between the EP and lamina propria (LP) layers, disappears. The differentiation between MiD and MoD is important because if a therapy is not applied for lesions more severe than MiD, these lesions may be prone to develop into an SCC. In other words, an MiD lesion can naturally recover to normal if the patient stops the harmful habits, such as smoking and betel nut chewing. However, beyond the stage of MiD, a medical treatment is usually needed. In the conventional diagnosis procedure, biopsy is used for obtaining histological

#165178 - $15.00 USD Received 21 Mar 2012; revised 29 May 2012; accepted 14 Jun 2012; published 18 Jun 2012
(C) 2012 OSA

images. Judging from the distribution and number of dysplastic cells in the EP layer, we can make the diagnoses of MiD, MoD, severe dysplasia, and carcinoma *in situ*.

Optical coherence tomography (OCT) has been proved to be a useful technique for oral disease diagnosis [5–18]. In particular, based on the scanning images of a swept-source OCT system, a few effective diagnosis indicators for oral cancer and precancer have been identified [15–17]. These indicators include the EP layer thickness and the standard deviation (SD) of OCT signal intensity. In an abnormal oral EP containing dysplastic cells, the cell size, shape, nucleus size, and arrangement become more randomly distributed, when compared with healthy oral EP [4]. In this situation, light scattering becomes stronger and its spatial distribution becomes more strongly fluctuated. The light scattering behaviors are recorded in the spatial variations of OCT signal intensity. It is noted that the spatially average scattering intensity in a dysplastic oral EP is generally higher than a normal oral EP such that the corresponding average OCT signal intensity is relatively higher. Therefore, although the overall signal intensity may vary from one OCT image to another, the SD value without the normalization with respect to the average can better describe the rough morphology in a dysplastic oral EP. A normalization procedure will significantly blur the feature of stronger OCT intensity fluctuations in space. Statistics based on clinical practice has shown the high sensitivity and specificity in using those diagnosis indicators [16]. The SD calculation has also been used for diagnosing submucous fibrosis [18]. In such a diagnosis, the decrease of the SD level in the LP layer due to collagen deposition is observed. However, for the diagnosis of oral precancer, the increase of the SD value in the EP layer due to the existence of dysplastic cells is of our concern in this study.

In this paper, we demonstrate an effective OCT image analysis procedure for illustrating the important features of oral precancers, particularly MiD and MoD. We first use the proposed procedure for analyzing the histological images obtained from biopsy to show the reasonable key parameters of the conventional diagnosis method. The results from histological image analysis indicate the reasonable use of SD mapping for identifying the distribution of dysplastic cells in the EP layer near the EP/LP boundary. Then, the proposed analysis procedure with empirical parameters is applied to OCT images of different oral mucosal lesions for plotting the EP/LP boundary and evaluating the distribution of dysplastic cells in the EP layer. The SD mapping on an OCT image is performed using the raw data of OCT signal. OCT images obtained from clinical scanning on patients of various precancerous conditions are processed for evaluating the diagnosis statistics based on the optimized SD threshold for differentiating the MiD condition from the MoD stage. In section 2 of this paper, the OCT operation condition and oral mucosal samples are described. The analysis results of histological images are shown in section 3. Then, the approach for plotting the air/tissue and EP/LP boundaries is introduced in section 4. Next, the evaluation criteria and the statistical results in differentiating MoD from MiD are discussed in section 5. Finally, conclusions are drawn in section 6.

2. Method and samples

A swept-source OCT system is used for clinical scanning. In this system, a sweeping-frequency laser source with the output spectral peak at 1310 nm is used as the light source (Santec, HSL-2100-ST). The light source is connected to a Mach-Zehnder interferometer, which consists of two optical couplers and two circulators. The interference fringe signal is detected by a balanced photo-detector (Thorlabs, PDB450C-AC) and sampled by a high-speed digitizer (National Instruments). A probe with B-mode scanning based on a stepping motor-driven (Haydon, Captive 2800 Series) translation motion is connected to the OCT system for clinical scanning. The achieved system sensitivity and axial resolution in tissue are 103 dB and 6 μm (in tissues) at the depth of 1 mm, respectively. The lateral resolution is about 7 μm. It takes about 0.1 s to complete a two-dimensional image of 1.3 cm in lateral dimension. Other details about the OCT system and operation can be found in [16].

OCT images for analysis were collected from clinical scanning of patients at their visits to the National Taiwan University Hospital. Totally 137 buccal mucosa OCT images with the

#165178 - $15.00 USD Received 21 Mar 2012; revised 29 May 2012; accepted 14 Jun 2012; published 18 Jun 2012
(C) 2012 OSA

lateral dimension of 9.5 mm in each image from 54 patients were obtained for analysis, including 24 MiD and 30 MoD patients. The MiD and MoD diagnoses were made based on the interpretation of histological images. An OCT scanning image from the normal oral mucosa near the lesion of each patient was obtained for comparison. On the lesions of larger sizes in 15 MiD and 14 MoD patients, two OCT scanning images from two quite far-apart locations were acquired and are regarded as two different samples. For the remaining 9 MiD and 16 MoD patients, only one OCT image was obtained from each lesion. Therefore, 54 normal, 39 MiD, and 44 MoD OCT images in total are processed for evaluating the diagnosis statistics. It is noted that the OCT scanning location on the oral mucosa of a patient cannot be exactly the same as that of a biopsy. Therefore, the image contents of OCT scanning and histology cannot be the same even though the proposed analysis procedure for OCT and histological images can precisely reveal the individual features. For preparing the histological images, hematoxylin and eosin (H&E) stain was applied to the sections of biopsy oral samples. The images were taken with an Olympus microscope supplied with a digital camera (DP72, Olympus) at 100 × magnification.

3. Analyses of histology images

Figure 1(a) shows the histological image of healthy oral mucosa. Here, the purplish EP/LP boundary can be clearly seen. The JPEG (Joint Photographic Experts Group) file of the histological image (the raw data from a digital camera) is then processed with Labview software to convert the image into the intensity distributions of the three primary colors (RGB) with digitized maximum intensity at 255 and minimum intensity at 0 in each color. The blue and red dyes of H&E stain the cell nuclei and cytoplasm, respectively. To acquire a larger contrast between the cell nuclei and cytoplasm, we choose the intensity distribution of the red component for further analysis. The black and white image in Fig. 1(b) shows this red-color intensity distribution of the healthy oral mucosa in Fig. 1(a). The image has 2070 and 1548 pixels in the horizontal and vertical directions, respectively. Here, the dark spots correspond to cell nuclei. For SD mapping, a window of 20 pixels in the horizontal direction, corresponding to about 18 μm, and of one pixel in the vertical direction is used for evaluating the SD value. With the translational shift of the SD evaluation window pixel by pixel in both directions, we can obtain the SD mapping in the EP layer of the histological image, as shown in Fig. 1(c). The EP/LP boundary in Fig. 1(c) is manually plotted. Here, one can see that in almost the whole region of EP layer, the SD value is below 25.

Similar histological images for MiD and MoD oral mucosae are shown in Figs. 2 and 3, respectively. The MiD and MoD diagnoses are based on the dysplastic cell distributions indicated by the vertical bars, in which the blue and red portions correspond to the abnormal and normal parts of the EP, respectively, in Figs. 2(a) and 3(a), respectively. These two images are processed with the aforementioned procedures to give the intensity distributions of the red-color component in Figs. 2(b) and 3(b) and the SD mappings in Figs. 2(c) and 3(c), respectively. Here, one can see that in the EP layers of MiD and MoD lesions, SD values become larger (larger than 25) in certain regions. In particular, in Fig. 3(c) for the MoD case, the ranges of high SD values in certain portions almost reach the surface of the section of biopsy sample. Although from Figs. 2(c) and 3(c), it is difficult to confirm the diagnoses of MiD and MoD based on the extended range of high SD value distributions in the EP layers, the SD mapping results are essentially consistent with the diagnoses obtained from histological interpretation. The SD mapping may represent a powerful approach for assisting the histological interpretation. The SD mapping results in Figs. 2(c) and 3(c) clearly reflect the fact that the cell size, shape, nucleus size, and arrangement are more randomly distributed in the portions containing dysplastic cells. Such results imply that an OCT image, which is obtained based on light backscattering of tissue micro-morphology, should have the similar characteristics in spatial signal distribution. It is noted that in each of Figs. 1(c)-3(c), the SD mapping is shown only in the EP layer to draw the attention on the increased SD values in the EP layer due to the existence of dysplastic cells in the cases of MiD and MoD. The SD values in the LP layer are usually larger than those in the EP layer even though dysplastic cells exist.

#165178 - $15.00 USD Received 21 Mar 2012; revised 29 May 2012; accepted 14 Jun 2012; published 18 Jun 2012
(C) 2012 OSA

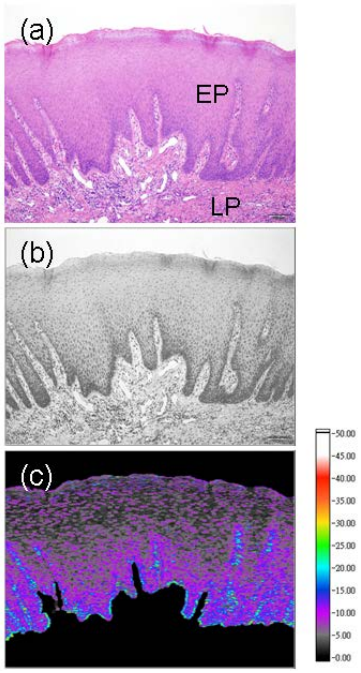

Fig. 1. Histological images of healthy oral mucosa with (a) for original image, (b) for the image of red component, and (c) for SD mapping in the EP layer.

4. Plotting boundaries in OCT images

Figure 4 shows the floating chart of the analysis procedure for OCT images. Before SD mapping in the EP layer, the air/tissue and EP/LP boundaries need to be reasonably plotted for defining the EP layer. Although the air/tissue and EP/LP boundaries can be clearly identified in an OCT image due to the large contrasts of signal intensity (dark in the air, bright in the EP layer, and even brighter in the LP layer) in an oral precancer sample, a computer program is needed to automatically plot the boundaries for real-time diagnosis. As shown in the floating chart, we first perform the SD mapping in the whole OCT image. In evaluating SD value, we use a window of 20 pixels (corresponding to 100 μm) in the lateral direction and one pixel in the depth direction for computation. With translational shift pixel by pixel in both directions, SD mapping can be implemented. In choosing the window size for SD evaluation in an OCT image, we have tried several sizes and found that the window of 20 x 1 pixel was an optimum selection. If the window is too small, it cannot reflect the statistical microstructure variations in the mucosa acquired by OCT scanning. However, if the window is too large, the SD mapping resolution becomes poor. It is noted that because the SD mapping in a histological image is simply to demonstrate the concept of SD mapping, it is unnecessary to select the same physical window size for SD mappings in a histological and an OCT image. From SD mapping, we can plot the air/tissue boundary quite precisely by connecting the vertical location in each A-mode scan, at which the SD value reaches 0.5 in tracing downward from the top of the image. Based on the analyses of all the recorded OCT images, the SD value in the air is always lower than 0.4. Therefore, the SD value of 0.5 is a good threshold for plotting the air/tissue boundary. The air/tissue boundary plotting based on this procedure is quite accurate as demonstrated by the red curve in either Fig. 5(a) or 5(b), in which an OCT image of MiD oral lesion is used as an image process example.

#165178 - $15.00 USD Received 21 Mar 2012; revised 29 May 2012; accepted 14 Jun 2012; published 18 Jun 2012
(C) 2012 OSA

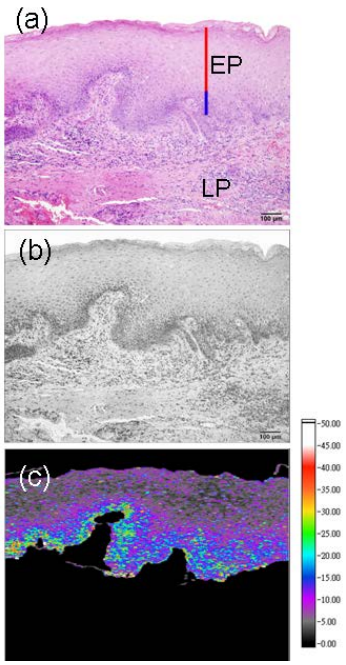

Fig. 2. Histological images of MiD oral mucosa with (a) for original image, (b) for the image of red component, and (c) for SD mapping in the EP layer. The MiD diagnosis is based on the dysplastic cell distribution indicated by the vertical bar in part (a), in which the blue and red portions correspond to the abnormal and normal mucosae, respectively.

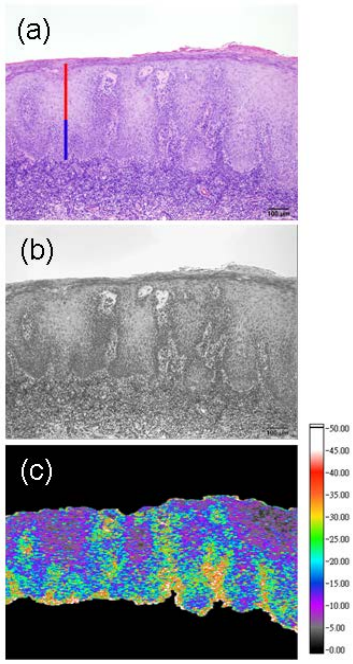

Fig. 3. Histological images of MoD oral mucosa with (a) for original image, (b) for the image of red component, and (c) for SD mapping in the EP layer. The MoD diagnosis is based on the dysplastic cell distribution indicated by the vertical bar in part (a), in which the blue and red portions correspond to the abnormal and normal mucosae, respectively.

#165178 - $15.00 USD Received 21 Mar 2012; revised 29 May 2012; accepted 14 Jun 2012; published 18 Jun 2012
(C) 2012 OSA

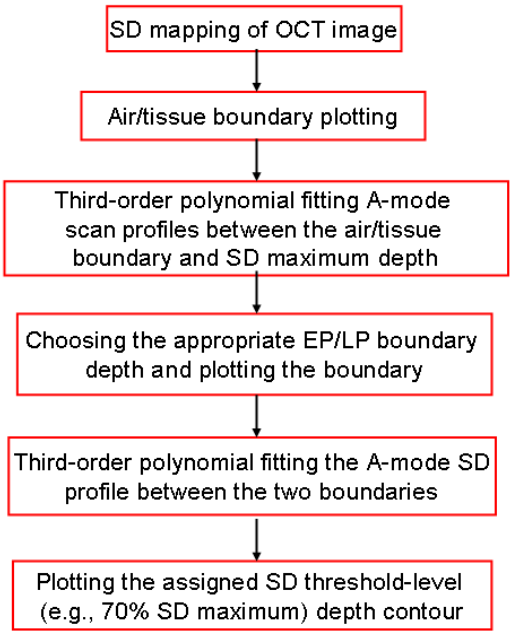

Fig. 4. Floating chart indicating the procedure of plotting the air/tissue boundary, the EP/LP boundary, the assigned SD threshold level contour in an OCT image.

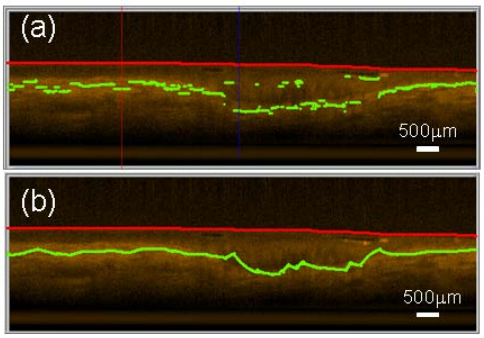

Fig. 5. (a) OCT image of a MiD oral mucosa sample with the contours of the air/tissue and EP/LP boundaries based on the criterion of SD = 0.5 and SD maximum, respectively. (b) The same OCT image with the boundaries smoothed by the modified moving average method.

The EP/LP boundary can also be roughly plotted by tracing the maximum level of SD value in each A-mode scan profile, as shown in the green curve of Fig. 5(a). Such a broken curve is connected by using the modified moving average technique [19–21] to give the rough EP/LP boundary in Fig. 5(b). However, significant discrepancies in quite many A-mode scans between the SD maximum depth and the real EP/LP boundary can be clearly seen. The left (red) and right (blue) vertical lines in Fig. 5(a) represent two A-mode scans of large and negligibly small discrepancies, respectively. The OCT signal intensity profiles between the air/tissue boundaries and the depths of SD maxima corresponding to the left and right vertical lines are shown in Figs. 6(a) and 6(b), respectively. Here, one can see that in the A-mode scan intensity profile of the small discrepancy between the EP/LP boundary and the depth of SD maximum (see Fig. 6(b)), the signal intensity fluctuations are relatively weaker, when compared with those in the A-mode scan intensity profile of large discrepancy (see Fig. 6(a)). In Fig. 6(a), the high intensity range actually belongs to the LP layer. In other words, the EP/LP boundary is mistakenly assigned by using the depth of SD maximum in this A-mode

#165178 - $15.00 USD Received 21 Mar 2012; revised 29 May 2012; accepted 14 Jun 2012; published 18 Jun 2012
(C) 2012 OSA

scan profile. It is noted that although the existence of dysplastic cells in the EP layer near the boundary may lead to enhanced OCT signal intensity in a certain range, its intensity level is still significantly lower than that in the LP layer. To obtain a more accurate EP/LP boundary point, the OCT intensity profile in Fig. 6(a) is fitted by a third-order polynomial to give the (red) smooth curve. We choose the depth, at which the fitted OCT intensity is double the average of the first 20 pixels right below the air/tissue boundary, as the new EP/LP boundary. The intensity level of the first 20 pixels and its double level are indicated by the two arrows in Fig. 6(a). It is noted that the similar third-order polynomial fitting in Fig. 6(b) does not lead to the finding of a depth, at which the fitted OCT intensity can be as large as double the average of the first 20 pixel. Therefore, we can build a general procedure of third-order polynomial fitting every A-mode scan intensity profile in the range between the determined air/tissue boundary and the depth of SD maximum. If a depth of double intensity as demonstrated in Fig. 6(a) is found, this depth is used for replacing the SD maximum location as the EP/LP boundary; otherwise, the depth of SD maximum is assigned as the EP/LP boundary. It is noted that the choice of doubling the average intensity of the first 20 pixels right below the air-tissue interface in finding the EP/LP boundary is based on two observations. First, the SD values in the LP layer are normally higher than two times those in the normal region of the EP layer. Second, in the cases of MiD and MoD, usually no dysplastic cell exists in the depth range of the first 20 pixels in the tissue.

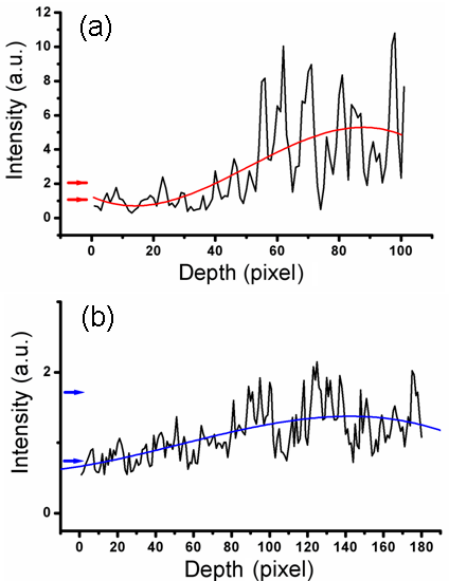

Fig. 6. A-mode scan profiles and their third-order polynomial fittings corresponding the left (red) (a) and right (blue) (b) vertical lines in Fig. 5(a). The arrows in each part indicate the intensity levels of the average of the first 20 pixels and its double level.

Following the procedure described above, the plot of SD maximum in Fig. 5(a) is modified to become the green curve in Fig. 7(a). This curve is then smoothed with the modified moving average method to give the green curve in Fig. 7(b). In this average method, five adjacent data points are averaged to give the new data value at the central point. Meanwhile, the data value of the point among the five with the largest deviation from the average level is replaced by the average value for the next averaging window along the curve. Although the green curve in Fig. 7(b) does not necessarily match completely the real EP/LP boundary, it is accurate enough for the diagnosis purpose and will be referred to as the EP/LP boundary. It is noted that in this OCT image, the EP layer thickness is always between 200 and 300 μm except the central portion, in which the EP layer thickness can be larger than 500

#165178 - $15.00 USD Received 21 Mar 2012; revised 29 May 2012; accepted 14 Jun 2012; published 18 Jun 2012
(C) 2012 OSA

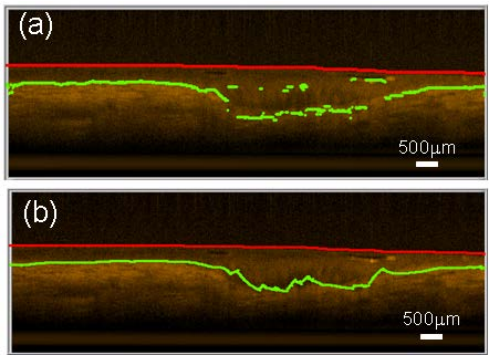

Fig. 7. (a) New plot of the EP/LP boundary after the correction based on the fitting in Fig. 6. (b) New EP/LP boundary contour smoothed by the modified moving average method.

μm. This OCT image came from a patient, who was diagnosed to have a MiD oral mucosal lesion. The thick EP layer in this portion represents one of the features for MiD diagnosis.

After the air/tissue and EP/LP boundaries are accurately plotted, a protocol needs to be built for determining the range of dysplastic cell distribution. As demonstrated in Figs. 2 and 3, the more irregular morphology of dysplastic cells leads to more strongly fluctuated OCT intensity distributions. Therefore, a procedure needs to be built for reasonably plotting the contour of an assigned SD threshold level in the EP layer. Figure 8(a) shows the contour of EP/LP boundary (the bottom green curve), the contour of 70% (an assigned SD threshold level) the SD level at the EP/LP boundary (the middle blue curve, which is very close to the EP/LP boundary), and the air/tissue boundary (the almost straight red line) in an OCT image of MoD oral mucosa. Here, the 70% contour obtained by connecting the corresponding depths in individual A-mode scans is unreasonable because the SD value fluctuates fast along depth. A more reasonable contour can be obtained by first fitting the A-mode scan SD variation with a third-order polynomial, as exemplified by the smooth curve in Fig. 8(b). Along the fitting curve, we can redefine the SD maximum level at the assigned EP/LP boundary, from which we can re-plot the contour of 70% SD maximum level. The new contour is shown as the blue curve in Fig. 8(c). It is interesting to observe that in the portion of thick EP layer of this OCT image, which came from a MoD patient, the depth range of 70% SD maximum level from the EP/LP boundary is also relatively larger, indicating the existence of dysplastic cells in a larger depth range of the EP layer. The procedure discussed above is outlined in the floating chart of Fig. 4.

5. Diagnosis results and discussions

Following the built procedure, we can process all the OCT images we recorded. Figures 9-11 show the analysis results of a healthy oral mucosa case, a MiD case, and a MoD case, respectively. In each figure, part (a) shows the OCT image, part (b) demonstrates the SD mapping, and part (c) illustrates the OCT image together with the plotted contours, including (from top to bottom) the air/tissue boundary (the red curve), the 70% SD maximum level contour (the blue curve), and the EP/LP boundary (the green curve). For the discussions later, as shown in Figs. 9(c), 10(c), and 11(c), we define a parameter D as the thickness percentage of the high SD-level range (between the blue and green curves) in the whole EP layer (between the red and green curves) of an A-mode scan line when an SD threshold level is assigned (70% the maximum SD level in Figs. 9-11). In other words, D is regarded as the range percentage of dysplastic cell distribution in the whole EP layer along an A-mode scan of a MiD or MoD sample. The same D parameter is defined for a normal sample even though no dysplastic cell exists in such a sample. Due to the rough interface structure between the EP and LP layers, high SD values are obtained near the EP/LP boundary. Based on the definition of D, we also define D_{ave} as the laterally average D value of an OCT image. It is noted that the high SD values in the EP regions assigned for the dysplastic cell distributions in Figs. 9(c)-

#165178 - $15.00 USD Received 21 Mar 2012; revised 29 May 2012; accepted 14 Jun 2012; published 18 Jun 2012
(C) 2012 OSA

11(c) are lower than the SD levels in the LP layers. In an OCT image, the SD level in the LP layer is usually higher than that in the EP layer no matter whether dysplastic cells exist in the EP layer.

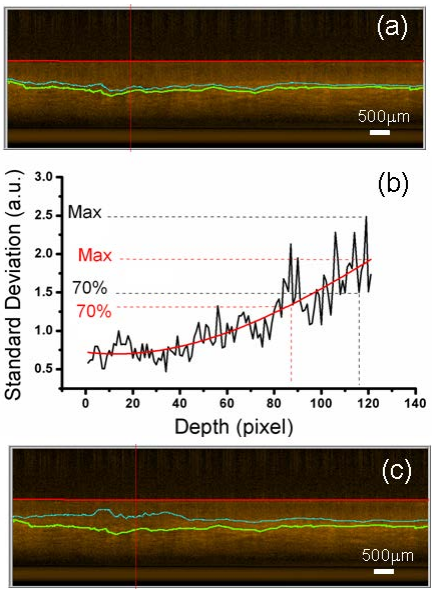

Fig. 8. (a) OCT image of a MoD oral mucosa sample with the contours of the air/tissue boundary, the EP/LP boundary, and the contour of 70% SD maximum level in the EP layer. (b) The SD variation profile along the A-mode scan indicated by the vertical line in part (a) and its third-order polynomial fitting curve. (c) The same OCT image as that in part (a) except that the contour of 70% SD maximum level in the EP layer is re-plotted based on the third-order polynomial fitting like the smooth curve shown in part (b).

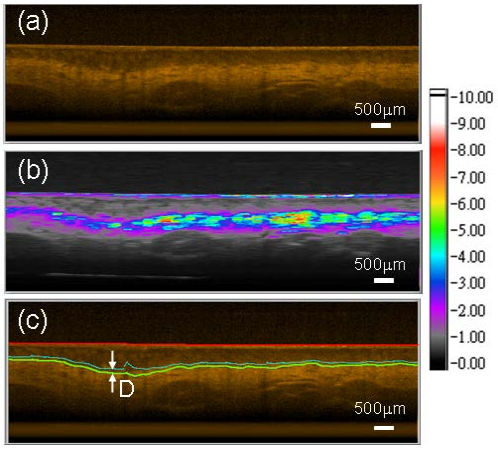

Fig. 9. OCT images with the analysis results of a healthy oral mucosa case, including (a) for the original OCT image, (b) for demonstrating the SD mapping, and (c) for illustrating the OCT image together with the plotted curves (from top to bottom) of the air/tissue boundary (the red curve), the 70% SD maximum level contour (the blue curve), and the EP/LP boundary (the green curve). D is defined as the thickness percentage of high SD-level range (between the blue and green curves) in the whole EP layer (between the red and green curves) of an A-mode scan line when an SD threshold level is assigned.

#165178 - $15.00 USD Received 21 Mar 2012; revised 29 May 2012; accepted 14 Jun 2012; published 18 Jun 2012
(C) 2012 OSA

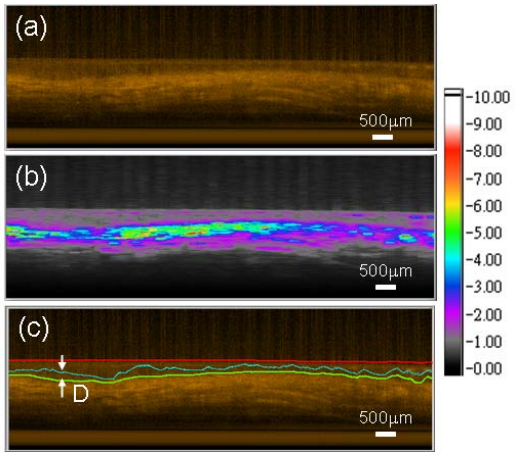

Fig. 10. Similar to Fig. 9 except for a MiD case.

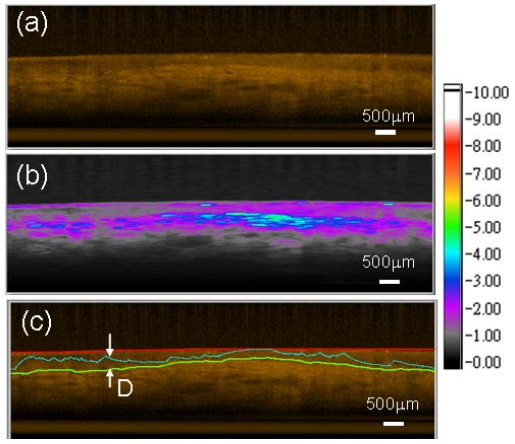

Fig. 11. Similar to Fig. 9 except for a MoD case.

Figure 12 shows the data distribution of D_{ave} when the SD threshold for dysplastic cell distribution is set at 70%. In this figure, 137 data points, including 54 normal, 39 MiD, and 44 MoD OCT images, are included. In Fig. 13, three receiver operating characteristic (ROC) curves for differentiating MiD from normal with various D_{ave} criteria are plotted. Here, the black continuous, blue dash-dotted, and red dashed curves correspond to the conditions of 65, 70, and 75% in SD threshold level, respectively. The D_{ave} criterion varies from ~54, ~51, and ~50% at the left ends through ~11, ~8, and ~7% at the right ends in the curves of 65, 70, and 75% in the SD threshold level, respectively. In those curves, a data point closest to the upper-left corner of the figure represents the optimum condition of high sensitivity and specificity for selecting the D_{ave} criterion and SD threshold level. In Fig. 13, a circular arc centered at the upper-left corner is drawn to touch the curve of 70% in SD threshold level at a point of 24% in D_{ave} criterion, which corresponds to the optimum condition for differentiating MiD from normal. Under this condition, the sensitivity and specificity for differentiating MiD from normal are about 64 and 69%, respectively. Such values for sensitivity and specificity are quite low, indicating the difficulty of differentiating MiD from normal based on the proposed method. Figure 14 shows the ROC results, similar to Fig. 13, for differentiating MoD from normal. Again, the black continuous, blue dash-dotted, and red dashed curves correspond to the conditions of 65, 70, and 75% in SD threshold level, respectively. The D_{ave} criterion varies from ~54, ~51, and ~50% at the left ends through ~32, ~23, and ~19% at the right ends in the curves of 65, 70, and 75% in the SD threshold level, respectively. In Fig. 14, a circular arc

#165178 - $15.00 USD Received 21 Mar 2012; revised 29 May 2012; accepted 14 Jun 2012; published 18 Jun 2012
(C) 2012 OSA

centered at the upper-left corner is drawn to touch the curve of 75% in SD threshold level at a point of 35% in D_{ave} criterion, which corresponds to the optimum condition for differentiating MoD from normal. Under this condition, the sensitivity and specificity for differentiating MoD from normal are about 92 and 94%, respectively. Such high values of sensitivity and specificity imply that the differentiation between MoD and normal is relatively easier.

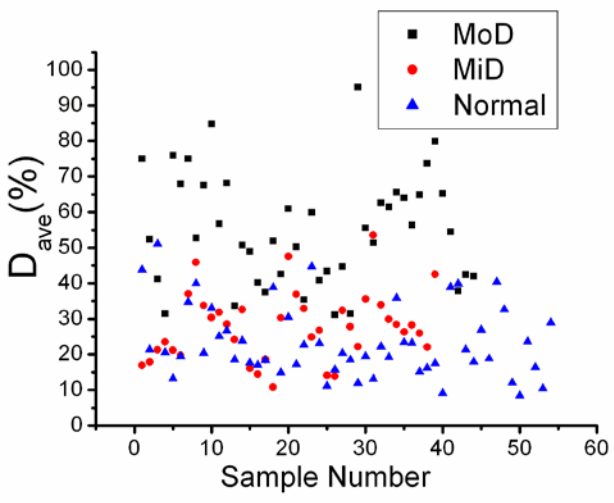

Fig. 12. Data distribution of D_{ave} when the SD threshold for dysplastic cell distribution is set at 70%. Here, 137 data points, including 54 normal, 39 MiD, and 44 MoD OCT images, are included.

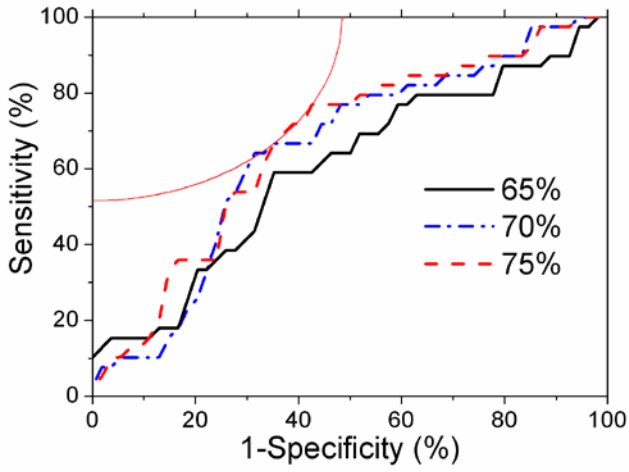

Fig. 13. Three ROC curves for differentiating MiD from normal with various criteria of D_{ave}. Here, the black continuous, blue dash-dotted, and red dashed curves correspond to the conditions of 65, 70, and 75% in SD threshold level, respectively. A circular arc centered at the upper-left corner is drawn to touch the curve of 70% in SD threshold level at a point of 24% in D_{ave} criterion for indicating the optimum conditions.

Based on our SD mapping approach, there is a certain D value in an A-mode scan of a normal sample (see Fig. 9(c)) even though no dysplastic cell distribution exists. Also, the D_{ave} value of a normal sample may vary among different patients. To take these factors into account, we use the difference of D_{ave} between either a MiD or MoD sample and its individual normal sample of the same patient as the parameter for diagnosing the precancerous conditions. Also, because a medical treatment is usually not applied to a patient until the

#165178 - $15.00 USD Received 21 Mar 2012; revised 29 May 2012; accepted 14 Jun 2012; published 18 Jun 2012
(C) 2012 OSA

lesion evolves into the stage of MoD, we are mainly concerned with the differentiation between MiD and MoD. In Fig. 15, we plot the data points of the D_{ave} difference, including 39 MiD and 44 MoD OCT images. Here, one can see that the two groups of data point can be roughly differentiated. In Fig. 16, three ROC curves for differentiating MoD from MiD with various criteria of D_{ave} difference are plotted. Here, again, the black continuous, blue dash-dotted, and red dashed curves correspond to the conditions of 65, 70, and 75% in SD threshold level, respectively. The criterion of D_{ave} difference varies from ~20% at the left ends through ~5% at the right ends in all the three curves of different SD threshold levels. In Fig. 16, a circular arc centered at the upper-left corner is drawn to touch the curve of 70% in SD threshold level at two points of 13 and 16% in D_{ave} difference criterion. Under the condition of 13 (16) % in D_{ave} difference criterion, the sensitivity and specificity for differentiating MoD from MiD are around 82 (80) and 90 (97) %, respectively.

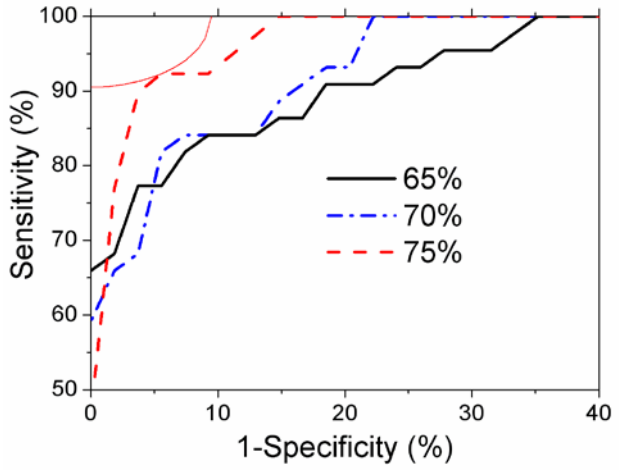

Fig. 14. Three ROC curves for differentiating MoD from normal with various criteria of D_{ave}. Here, the black continuous, blue dash-dotted, and red dashed curves correspond to the conditions of 65, 70, and 75% in SD threshold level, respectively. A circular arc centered at the upper-left corner is drawn to touch the curve of 75% in SD threshold level at a point of 35% in D_{ave} criterion for indicating the optimum conditions.

The proposed image analysis procedure can be used only when the EP/LP boundary still exists in the oral mucosa under examination. Beyond the stage of carcinoma *in situ*, this boundary disappears. In this situation, the SD maximum contour may still exist; however, it does not represent the EP/LP boundary. Under this condition, visual examination of an OCT image before image analysis is needed for differentiating the precancerous from cancerous lesions. Even a sophisticated computer program is built for effectively evaluating the oral mucosa condition, a quick visual examination is still needed for understanding the general situation of the examined mucosa.

The required period for completing the analysis procedure of one OCT image is about 2 sec. Suppose at a visit of a patient, ten OCT images are to be acquired, which needs the scanning time of a few tens sec (0.1 sec of real scanning time for one image). The required period for OCT scanning and image analysis will be shorter than a couple min. With the analysis data, a medical doctor can make the diagnosis of an oral lesion in a few min. Therefore, almost real-time diagnosis of an oral precancer becomes possible.

#165178 - $15.00 USD Received 21 Mar 2012; revised 29 May 2012; accepted 14 Jun 2012; published 18 Jun 2012
(C) 2012 OSA

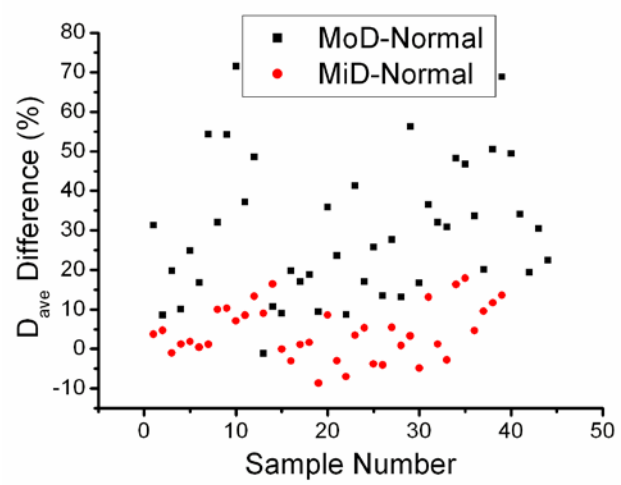

Fig. 15. Data distribution of the D_{ave} difference between either a MiD or MoD sample and its individual normal sample of the same patient when 70% is chosen for the SD threshold level.

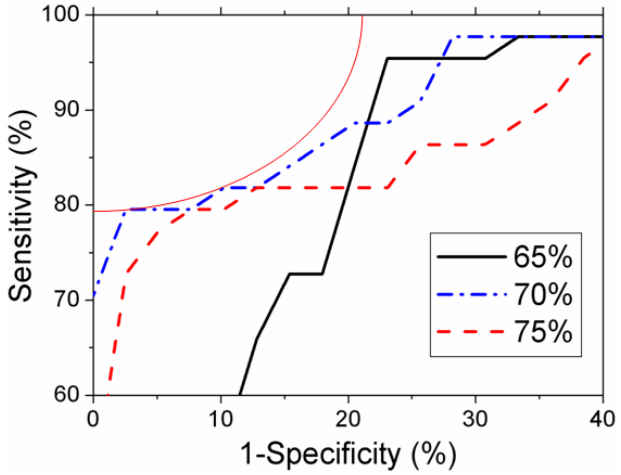

Fig. 16. Three ROC curves for differentiating MoD from MiD with various criteria of D_{ave} difference. Here, the black continuous, blue dash-dotted, and red dashed curves correspond to the conditions of 65, 70, and 75% in SD threshold level, respectively. A circular arc centered at the upper-left corner is drawn to touch the curve of 70% in SD threshold level at two points of 13 and 16% in D_{ave} difference criterion for indicating the optimum conditions.

6. Conclusions

In summary, a computer analysis procedure for an OCT image of healthy and precancerous oral mucosa has been demonstrated to reasonably plot the EP/LP boundary, determine the EP thickness, and estimate the range of dysplastic cell distribution based on SD mapping. Due to the more random variations of cell size, shape, nucleus size, and arrangement in dysplastic cell distribution, light scattering led to more strongly fluctuated intensity distribution in space, as illustrated by the intensity SD evaluation in a histological image. Therefore, the SD of OCT signal intensity could be used to calibrate the distribution range of dysplastic cells in the EP layer. Based on SD mapping in an OCT image, it was found that the laterally average range percentage of 70% SD maximum level in the EP layer could be a reasonably good threshold for differentiating MoD from MiD based on OCT image analysis. The sensitivity and specificity in diagnosis statistics could reach 82 and 90%, respectively.

#165178 - $15.00 USD Received 21 Mar 2012; revised 29 May 2012; accepted 14 Jun 2012; published 18 Jun 2012
(C) 2012 OSA

Because the OCT scanning and image analysis for a patient could be completed within a few min, almost real-time diagnosis of an oral precancer based on OCT scanning becomes possible. The proposed OCT image analysis method is currently used for clinical test in our University Hospital. Collection of more lesion cases is under way for obtaining more accurate statistics in using OCT scanning for oral precancer diagnosis.

Acknowledgments

This research was supported by the National Science Council and National Health Research Institute, Taiwan, The Republic of China, under the grants of NSC 100-2218-E-002-003, NSC 99-3114-B-002-005, and NHRI-EX101-10043EI.

#165178 - $15.00 USD Received 21 Mar 2012; revised 29 May 2012; accepted 14 Jun 2012; published 18 Jun 2012
(C) 2012 OSA